IEEE Access
Multidisciplinary | Rapid Review | Open Access Journal

Received November 1, 2019, accepted December 5, 2019, date of current version December 26, 2019.

Digital Object Identifier 10.1109/ACCESS.2019.2958981

New Method and Experiment for Detecting Relative Position and Posture of the Hydraulic Support

YI ZHANG[1], HONGYANG ZHANG[1], KUIDONG GAO[1], WENBO XU[1], AND QINGLIANG ZENG[1,2]

[1]College of Mechanical and Electronic Engineering, Shandong University of Science and Technology, Qingdao 266590, China
[2]College of Information Science and Engineering, Shandong Normal University, Jinan 250358, China

Corresponding author: Kuidong Gao (gaokuidong22@163.com)

This work was supported in part by the Key Research and Development Project of Shandong Province under Grant 2018GGX103027, in part by the National Natural Foundation of China under Grant 51974170, and in part by the Applied Basic Research Project of Source Innovation Program in Qingdao under Grant 18-2-2-20-jch.

ABSTRACT Hydraulic support is an indispensable equipment for coal mining face. To detect the position and posture of the hydraulic support and automatically control its straightness at the mining working face, we developed a device based on the principle that three noncolinear points determine a plane and proposed a novel method using it. First, the sensor parameters in the device were experimentally calibrated. Second, the accuracy of the device was evaluated in the single point detection experiment by measuring the position of the nine datum points. Through actual testing, our detection accuracy can reach 24.82mm. Third, our method was validated in the experiment of the plane detection. Finally, the detection device was installed on the hydraulic support mode. The change of the position and posture of the canopy in the movement of the hydraulic support lifting leg, realized the detection of position and posture of the adjacent hydraulic support, and the feasibility of the detection method was verified. Our research on the position and posture detection of the hydraulic support can lay an important theoretical foundation for the automatic control of the straightness of mining working face and the surveillance of the dangerous posture of the hydraulic support. Furthermore, it can provide a novel monitoring approach for preventing collapse of hydraulic supports under complex geological conditions such as large dip angles and large mining heights.

INDEX TERMS Hydraulic support, mining working face, detection device, position and posture detection, straightness detection.

I. INTRODUCTION

A. BACKGROUND

China is the largest energy consumer in the world. Coal is still China's main energy source, occupying more than 60% of the total energy consumption. Therefore, underground coal automation and intelligent mining technology is an inevitable trend for coal mining technology development [1].

The hydraulic support is the key equipment for the fully mechanized mining face [2], [3]. Two important parameters for the operation of mining working face are the straightness of the hydraulic support group and the posture of the hydraulic support. The coal mining efficiency is determined by the working performance of the hydraulic support and the degree of auto-straightening of the mining working face. The stability of hydraulic supports is difficult due to the complicated geological conditions of large dip angle, thick and extra-thick coal seams. The arrangement model of the hydraulic support in different postures is shown in Fig. 1. At present, the length of fully mechanized mining face in China is generally 120 m-300 m. Ideally, the hydraulic supports are distributed in a straight line on mining working face, and their posture are close to each other, as shown in Fig. 1-a. However, due to the adverse underground working environment and the lifting and lowering of the leg, the hydraulic support may deviate from the ideal arrangement, and the relative posture will be rolled, twisted, or pitched, etc. And the hydraulic support groups will no longer maintain a straight-line

The associate editor coordinating the review of this manuscript and approving it for publication was Di He.

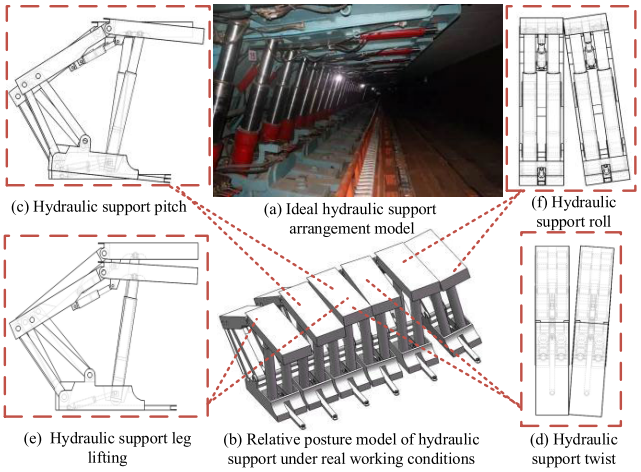

FIGURE 1. Arrangement model of the hydraulic support in different postures.

distribution, as shown in Fig. 1-b to 1-f. With existing technology, the operator is unable to obtain the real working state and posture of the whole hydraulic support, or reveal the time-coordinate relationship between the hydraulic support and the dynamic change process of the base and the canopy posture. Conventionally the hydraulic support positioning is usually adjusted by pulling the rope on mining working face manually or by infrared beam, such a method does not meet the requirements for automation of the fully mechanized mining face, nor does it guarantee accuracy, which greatly affects the mining efficiency and the safety of the coal mine.

B. RELATED WORKS

In attempts to automate the fully mechanized mining face, the coal mining machine positioning problem was solved by the geographic information system and the inertial navigation technology [4]. In 2016, Luo and Fan *et al* proposed a shearer wireless positioning method under the conditions of inaccurate anchor nodes, evaluated the accuracy of the shearing machine positioning and performed a comprehensive experiment of node configuration by using the memory cutting technology [5]. Mining working face is required to maintain a certain straightness and realize the automation and intelligent control of the hydraulic support in order to ensure the normal walking of the shearer in the long wall mining process [6], [7]. In 2017, Hao and Wang *et al* constructed the track geometry measurement model of the scraper conveyor according to the position of the shearer, They proposed the method of measuring the straightness of the scraper conveyor using the inertial measurement unit and the axial encoder, and tested the measurement using the longwall mining surface model [8]. The above research provided theoretical guidance and technical support for the positioning monitoring of coal mining face equipment and the straightening of mining working face, which lays a foundation for the automatic control of mining working face.

Considering the complex and uncertain environment of coal mines, automation equipments need to cope with various uncertain situations. With the development of automation technology, there are two main methods for detecting and controlling the straightness of mining working face. One is to control the straightness of mining working face by controlling the straightness of the scraper conveyor, and the other is to maintain the straight line of mining working face by controlling the position, posture, and straightness of the hydraulic support. In 2017, Wang, Wang, and Xu *et al* proposed a method for measuring the movement distance of hydraulic support based on machine vision in view of the inaccurate and unreliable measurement. Good measurement results were obtained during the experimental phase [9]. In 2018, Meng and Zeng *et al* analyzed the main factors of the failure of the hydraulic support by establishing a mathematical model of the bearing capacity of the hydraulic support under various load conditions, and proposed an optimization method of the support structure [10]. This study lays a theoretical foundation for the analysis of stent posture and the prevention of instability of the stent. In 2018, Meng and Zeng *et al* developed a posture controller based on electromechanical-liquid coordination technology to accurately monitor and control the posture of the hydraulic support [11]. In 2018, Liang and Fang *et al* proposed an error compensation method for tilt detection, and designed a fiber Bragg grating tilt sensor to monitoring the posture of the hydraulic support online [12]. In 2019, Xie, Jia, and Wang *et al* developed a posture-aware method for a hydraulic support group in a virtual reality environment by installing a tilt sensor on the base, front, rear link or canopy to obtain data. By comparing the predicted data with the actual data, the mining working status of the hydraulic support can be obtained [13].

Although the above related theories have been verified experimentally, most of these methods are difficult to be applied to the coal mining face due to the harsh working environment. There is much dust and low visibility in coal mines, many new types of equipment can not be used in mines. The positioning method based on the shearer or scraper conveyor can reflect the straightness of the mining working face, but it cannot reflect the status of the hydraulic support and further reveal the working condition of the hydraulic support group. Moreover, most of the above methods are only addressing either the working state of the equipment or the straightness of mining working face, but do not integrate both factors together.

The first step to improve the automation level of mining working face is still to determine the relative position and posture of the hydraulic support. This will prevent the support from acquiring dangerous postures such rolling and twisting, and in turn establish the basis of the automatic control of the straightness of mining working face.

C. MOTIVATION FOR OUR WORK

In this paper, a method for detecting relative position and posture was proposed based on the idea that three points can determine a plane. First, the relative position and posture of two adjacent hydraulic supports was detected. The space

six-degree-of-freedom detection can be extended to all hydraulic supports of mining working face. At present, the dynamic spatial position measurement method and the six-degree-of-freedom posture detection are mostly used in the field of positioning with robot technology and numerical control machine tools [14], [15]. The detection method proposed in this paper has rich and accurate mathematical expression of the relative position and posture of the hydraulic support, which can achieve the full pose analysis of the hydraulic support. At the same time, the position and posture detection method used in this paper is contact measurement, which has high reliability and can overcome the harsh environment of coal mines.

The research on relative position and posture detection lays a foundation for the analysis of the straightness of mining working face and the dangerous posture of the hydraulic support. The significance of the position and posture detection of the hydraulic support lies not only in the need for the straightness control of the hydraulic support, but also in the feedback of the status of the roof. It is a major technical breakthrough to improve the existing detection methods of the hydraulic support and the automation level of mining working face straightening. The progress in the development of the instability detection, the automatic prevention, and control technology of the hydraulic support during the mining process of large dip angle and large mining height coal seam has taken a solid step forward in China.

D. ORGANIZATION OF THIS PAPER

The remainder of this paper is organized as follows. In Section II, we described the principle of relative position and posture detection and established a mathematical model. In Section III, we conducted the design and development of the inspection system. In Section IV we selected and calibrated the sensor parameters. In Section V, we performed experimental measurements and evaluate the accuracy of the test. In Section VI, we came to the conclusion.

II. PRINCIPLE AND MATHEMATICAL MODEL OF DETECTION

There are movement actuators such as legs and equilibrium jacks in the hydraulic support, and their positions and postures will change with the needs of the support work [16]. The schematic diagram of the hydraulic support and relative position and posture detection device is shown in Fig. 2. When establishing the relative pose detection model, the change of the posture of the hydraulic support itself is temporarily ignored, and the hydraulic support is abstracted into a plane in the space.

The basic principle of relative position and posture detection is shown in Fig. 3. The two adjacent hydraulic supports were abstracted into two planes, which are defined as ''Reference hydraulic support plane'' and ''Pending detection hydraulic support plane''. The coordinate system o-xyz was fixed on the plane of the reference hydraulic support, and three fixed points P, A, and B were taken on the plane of

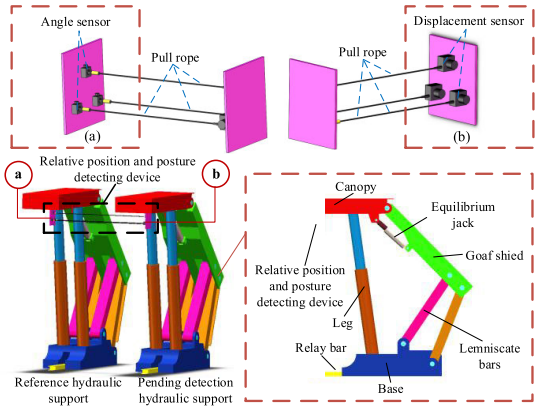

FIGURE 2. Schematic diagram of hydraulic support, position and posture detection device.

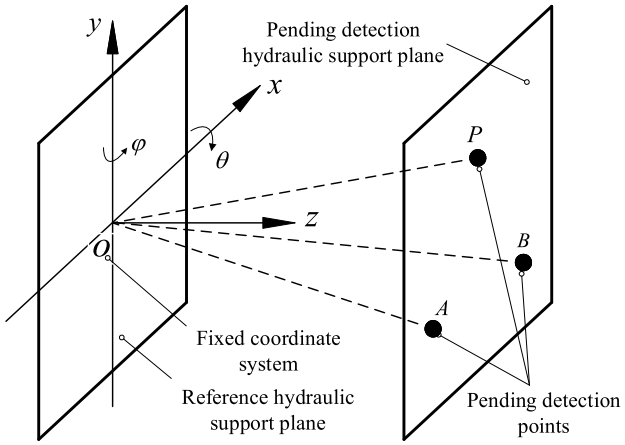

FIGURE 3. Basic schematic diagram of relative position and posture detection.

the hydraulic support to be tested, and the coordinate values of the three points in the coordinate system o-xyz were measured. The principle of determining the plane from three points obtains the position and posture of the plane to be measured in the coordinate system o-xyz. In practical applications, the relative position and posture detection device is mounted on the canopy of the hydraulic support (the canopy is abstracted into a plane), and the relative posture of the canopy is detected to further analyze the relative posture of the hydraulic support.

The key to the above method is how to obtain the coordinates of the three points P, A and B in the coordinate system o-xyz. In this paper, we present a method combining direction angle and vector length to obtain the coordinates of the point. The principle of spatial point coordinate detection is shown in Fig. 4. Taking the coordinates of point P as an example, it is assumed that there is a point P at any position in the space (in practical application of the hydraulic support relative position and posture detection device, this point only appears on the side of the x-o-y plane where the positive z-axis is pointing), $\overrightarrow{oP}$ can be obtained in the coordinate system o-xyz. The angle between the projection of the $\overrightarrow{oP}$ in the y-o-z plane and the positive direction of the z-axis was defined as θ, and the angle between the projection of the $\overrightarrow{oP}$ in the x-o-z plane

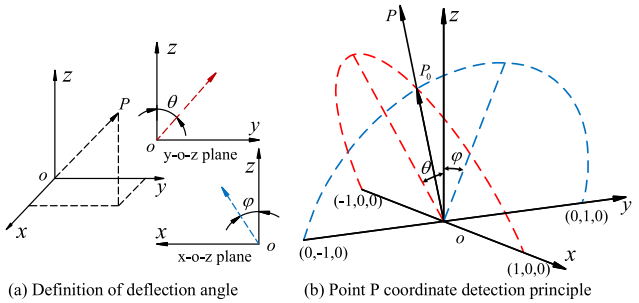

(a) Definition of deflection angle (b) Point P coordinate detection principle

FIGURE 4. Principle of space point coordinate detection.

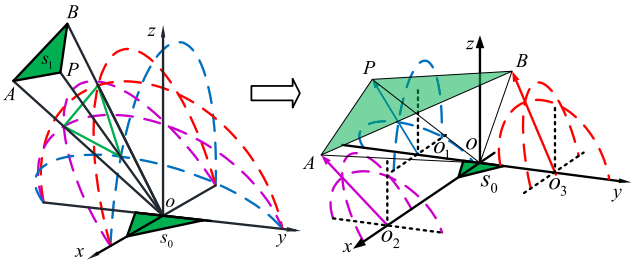

FIGURE 5. Comparison of the relative plane detection principle diagram in theory and in practice.

and the positive direction of the z-axis was defined as φ. The definition of the deflection angle is shown in Fig. 4-a. Further, according to the geometric relationship shown in Fig. 4-b, the formula of the point P coordinates can be obtained:

$$P=\begin{bmatrix}x_p\\y_p\\z_p\end{bmatrix}=l\cdot\begin{bmatrix}\cos(\arctan(1/\cos\theta\tan\varphi))\\-\sin\theta\sin(\arctan(1/\cos\theta\tan\varphi))\\\cos\theta\sin(\arctan(1/\cos\theta\tan\varphi))\end{bmatrix}\quad(1)$$

where x_p, y_p, and z_p are the coordinates of point P, and l is the distance of $\overrightarrow{oP}$.

According to the above principle, the coordinates of any point in the space can be obtained. The coordinates of three points can be acquired by obtaining a different θ and φ three times, a plane can be determined. The comparison between the principle diagram of the relative plane in theory and in practice is shown in Fig. 5. In the space, there were two planes of relative motion S_0 and S_1. First, the coordinate system o-xyz was established on the S_0, and points P, A, and B were selected on S_1, based on the above-mentioned spatial point detection principle. The three variables θ, φ, and l corresponding to the vectors $\overrightarrow{oP}$, $\overrightarrow{oA}$, and $\overrightarrow{oB}$ were measured respectively, and the coordinates of the three points P, A, and B can be calculated. The coordinates of the position and posture of the motion plane S_1 under the coordinate system o-xyz can be determined from the coordinates of the three points, and the relative position and posture of the two moving objects in the space can also be determined.

The angle sensor used in this experiment can not measure three different directions at the same point at the same time. It is necessary to measure three points with three angle sensors. Three angle sensors at o_1, o_2, and o_3 can be arranged and the coordinates of the points P, A, and B can be measured in the coordinate system with o_1, o_2, and o_3 as the origin according to each coordinate system and the fixed coordinate system o-xyz. The position and posture relationship will transform the measured coordinate values to a fixed coordinate system o-xyz.

Referring to Fig. 5, the coordinates of the points P, A, B are calculated as follows:

$$P=\begin{bmatrix}x_p\\y_p\\z_p\end{bmatrix}=l_1\cdot\begin{bmatrix}\cos(\arctan(1/\cos\theta_1\tan\varphi_1))\\-\sin\theta\sin(\arctan(1/\cos\theta_1\tan\varphi_1))\\\cos\theta\sin(\arctan(1/\cos\theta_1\tan\varphi_1))\end{bmatrix}+\Delta o_1\quad(2)$$

$$A=\begin{bmatrix}x_a\\y_a\\z_a\end{bmatrix}=l_2\cdot\begin{bmatrix}\cos(\arctan(1/\cos\theta_2\tan\varphi_2))\\-\sin\theta\sin(\arctan(1/\cos\theta_2\tan\varphi_2))\\\cos\theta\sin(\arctan(1/\cos\theta_2\tan\varphi_2))\end{bmatrix}+\Delta o_2\quad(3)$$

$$B=\begin{bmatrix}x_b\\y_b\\z_b\end{bmatrix}=l_3\cdot\begin{bmatrix}\cos(\arctan(1/\cos\theta_3\tan\varphi_3))\\-\sin\theta\sin(\arctan(1/\cos\theta_3\tan\varphi_3))\\\cos\theta\sin(\arctan(1/\cos\theta_3\tan\varphi_3))\end{bmatrix}+\Delta o_3\quad(4)$$

where Δo_1, Δo_2, and Δo_3 are $\overrightarrow{oo_1}$, $\overrightarrow{oo_2}$, and $\overrightarrow{oo_3}$, respectively.

Based on the principle of combining the direction angle and the vector length to obtain the coordinates of the spatial point, the relative position and posture detecting device is built by the combination of the angle sensor and the displacement sensor in the experiment to realize the measurement and calculation of the above parameters, and the corresponding parameters of each measuring point as shown in Table 1.

The single point detection experimental device is shown in Fig. 6. Fig. 6-a shows the combination of the angle sensor and the displacement sensor, which enables the detection of a point in space. Fig. 6-b is a physical diagram of the displacement sensor. The free end of the cable of the displacement sensor can reach any position in the space within the constraint of the length of the rope. When the free end is fixed at a certain point in the space, the scroll spring inside the sensor can ensure that cable is completely tensioned, and the distance from the free end to the outlet is the measured distance. Fig. 6-d shows the physical map of the angle sensor. The direction in which the coordinate axes of the coordinate system o-xyz point was marked: the z-axis was perpendicular to the angle sensor mounting plane and points to the direction of the point to be measured; the y-axis was vertically upward; and the x-axis orientation was determined based on the right-hand rule. This way to establish the coordinate system was used consistently throughout the experiments below.

III. DESIGN AND DEVELOPMENT OF DETECTION SYSTEMS

The sensor signal acquisition module designed in this paper is shown in Fig. 7. In this module, the minimum system board produced by a third-party manufacturer was selected [17]. The MCU used was STM32F407ZGT6 produced by ARM [18]–[20]. The module was externally

TABLE 1. Parameter naming corresponding to the measurement point.

Point	Coordinate	Deflection around the x-axis	Deflection around the y-axis	Modular length of vector
P	(p_x,p_y,p_z)	θ_1	φ_1	l_1
A	(a_x,a_y,a_z)	θ_2	φ_2	l_2
B	(b_x,b_y,b_z)	θ_3	φ_3	l_3

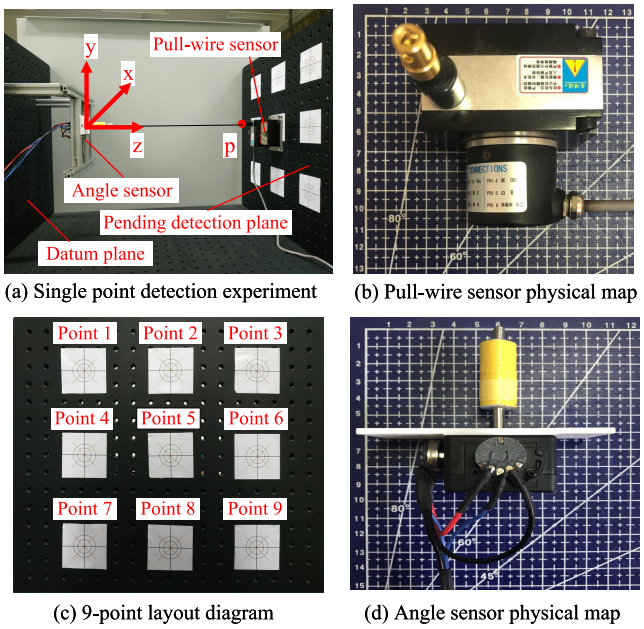

(a) Single point detection experiment (b) Pull-wire sensor physical map

(c) 9-point layout diagram (d) Angle sensor physical map

FIGURE 6. The single point detection experimental device.

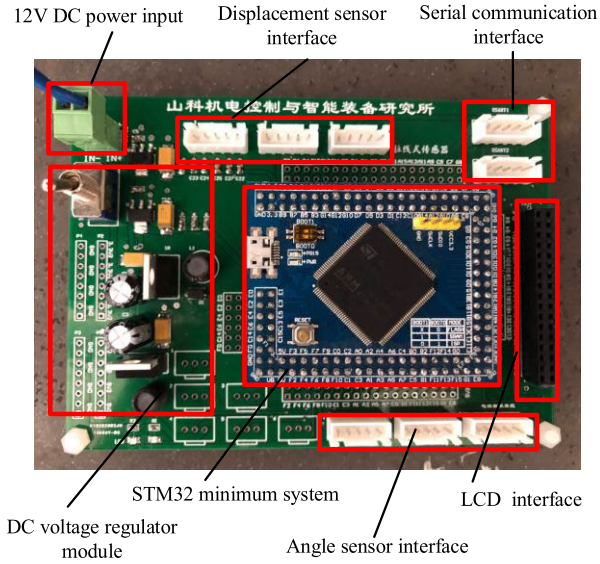

FIGURE 7. Sensor signal acquisition module.

connected with 12V DC power supply, 3 displacement sensors and 3 angle sensors. The CH340 chip was used to communicate with the PC. The LCD displayed the current collected data in real time and reported the current working status of the system. Signal acquisition and transmission

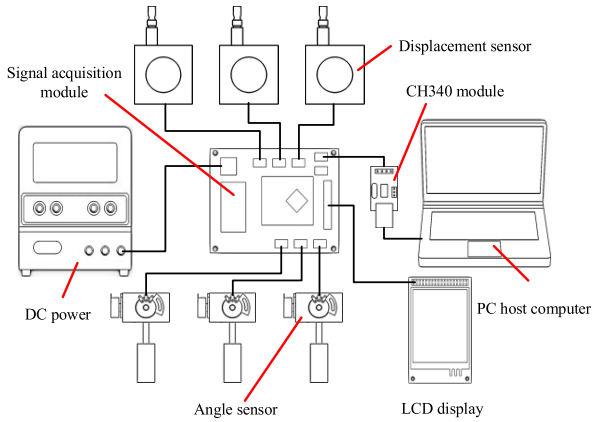

FIGURE 8. Signal acquisition and transmission system connection diagram.

system connection diagram is shown in Fig. 8. In the experimental stage, the sensor is powered by a 12V external DC power supply after voltage reduction; when it is later extended to the mining working face, a dedicated power module can be used to power the sensor alone.

The signal acquisition and data processing flow chart are shown in Fig. 9. The system sequentially collects the data of the displacement sensors and the angle sensors, and sends data to the PC through the serial port, and continuously refreshes the contents of the LCD screen during the transmission. Data transmission uses DMA channel, enabling high-speed sampling [21]. In MATLAB, the relevant parameters of the sensor are preset, and the acquired sensor data is substituted into the mathematical model of the spatial point coordinate solution, and the coordinate values of the points P, A, and B in the respective coordinate systems can be obtained.

The angle limit of the angle sensor used in the experiment was $\pm 25°$, and the accuracy of the sensor was calculated as $0.195°$. The experiment in this paper is based on single-point coordinates, and the procedure for coordinate transformation is not directly involved in the previous experiment.

IV. SENSOR PARAMETER SELECTION AND CALIBRATION

A. DISPLACEMENT SENSOR UNIT PULSE LENGTH CALIBRATION EXPERIMENT

The displacement sensor used in this paper converts the displacement signal of the cable into a digital pulse through an incremental encoder. The length of the cable corresponding to the single pulse of the sensor was experimentally determined. The displacement sensor selected for the experiment has a

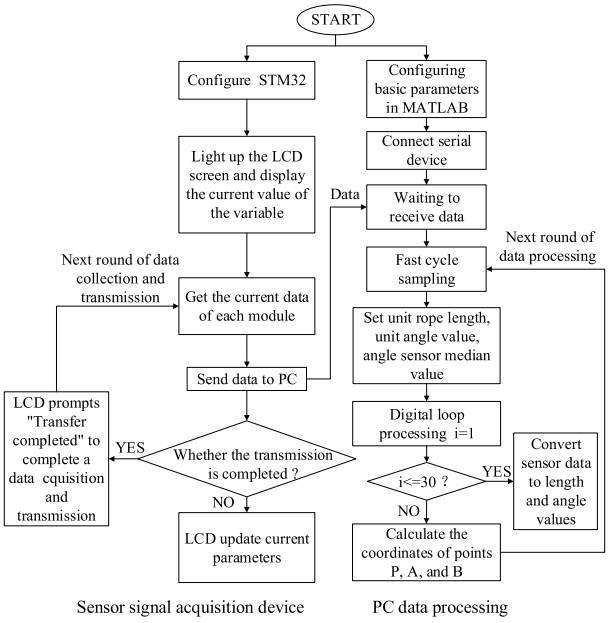

FIGURE 9. Sensor signal acquisition and data processing flow chart.

maximum extension length of 1500 mm, a maximum pull speed of 1 m/s, and 2000 pulses/rev.

The displacement sensor unit pulse corresponding length test experiment is shown in Fig. 10. In this experiment, the cable was pulled to the length of 100mm, 200mm, 300mm, 400mm, 500mm, and the number of pulses was recorded. The process was repeated 40 times in each group to eliminate experimental error, and the measurement results are shown in Fig. 10-a. The residual values in the sampling process are recorded simultaneously in Fig. 10-a. The mean of the number of pulses in each set of experiments were taken and a linear fit of the origin was performed to obtain the regression line of $y = 52.83x$, as shown in Fig. 10-b.

The analysis shows that the 40 sets of experimental results with the same elongation have high repeatability. Each extension of the pull cord is 1 mm, which corresponds to about 52.83 pulses, that is, the length of the corresponding pulse of the unit pulse is approximately 0.0189 mm. This parameter will be applied in mathematical models for solving spatial point coordinates. In addition, it should be noted that the three displacement sensors were shared in the experiment, and the parameter calibration methods for the other two sensors were the same as described. Since the displacement sensors used in the experiments were all produced by the same manufacturer, the respective values were almost equal by experiments.

B. ANGLE SENSOR NUMERICAL STABILITY EXPERIMENT

The angle sensor used in this paper uses a potentiometer to represent different position values in the mechanical structure as voltage signals. It converts and calculates the required angle values through the ADC. This experiment aims to collect the coordinates of a set of angle sensors and the cable to solve the space point in a relatively static state. The data

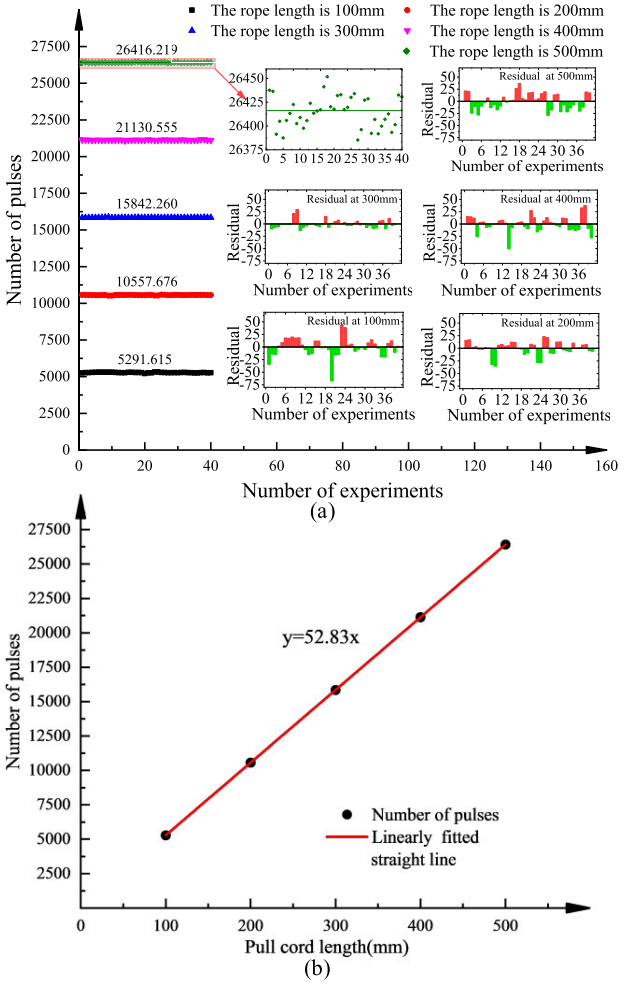

FIGURE 10. Displacement sensor unit pulse corresponding length test.

scatter plot of the angle sensor in the static state is shown in Fig. 11.

The analysis shows that there is numerical fluctuation in the sampling process. While the fluctuation of the z-axis value is relatively small, the fluctuation of the x-axis coordinate and the y-axis coordinate is relatively large. The fluctuation degree of the x-axis and the y-axis are close.

The z-axis direction is the direction to which the displacement sensor is connected, the value of the z-axis characterizes the length of the vector. The x-axis and y-axis directions are the directions connecting the angle sensors, the x-axis and y-axis characterize the direction angle of the vector. Therefore, if the same amount of change occurs, the z-axis fluctuation has a small effect, while the x-axis and y-axis values fluctuate greatly, the fluctuation trends are similar.

In order to determine the influence of numerical fluctuation on the detection accuracy, the numerical stability experiment of the angle sensor was carried out. In this experiment, one angle sensor and one displacement sensor were respectively fixed on two planes, and the two planes remained relatively static. The experimental device is shown in Fig. 6-a. The relative coordinates of the point P of the displacement

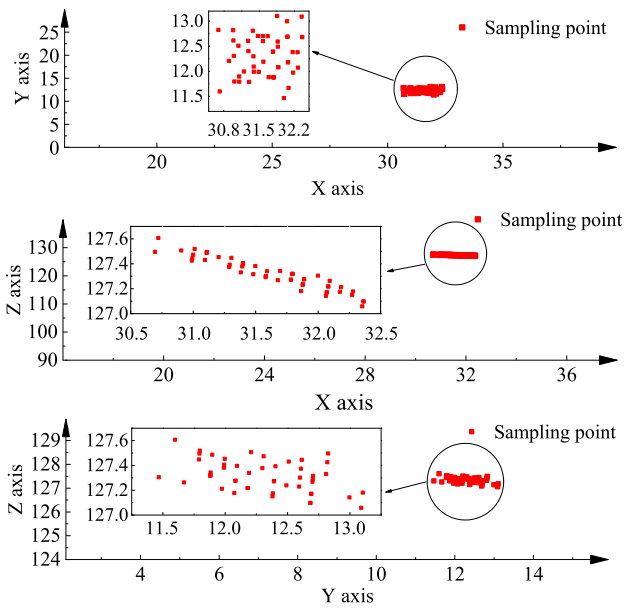

FIGURE 11. Data scatter plot of the angle sensor at rest.

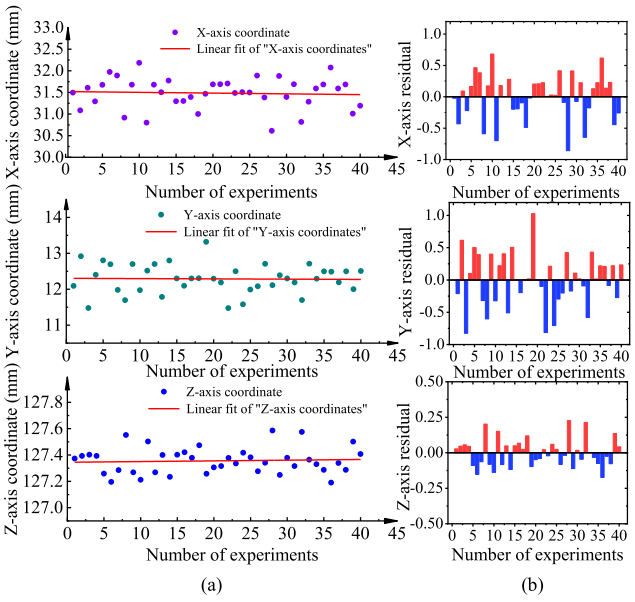

FIGURE 12. Single point position fixed multiple sampling experiment results.

sensor outlet were collected and calculated multiple times. The single-point position fixed multiple sampling experiment results are shown in Fig. 12. Fig. 12-a shows the results of a linear fit of 40 samples and Fig. 12-b shows the residuals for each sample.

Experiment shows that if a sufficient number of acquisitions are performed, when the slope is close enough to 0. And the regression curve can be considered to be a horizontal straight line, therefore the intercept can be determined as the coordinate value. However, within meeting the accuracy requirements, the sampling frequency should be reduced as much as possible to improve the response speed of the detecting device to the pose change. If the accuracy requirement is only within the mm level, the regression line intercept obtained from 20 samples is accurate enough to be taken as the coordinate of the point. If further accuracy is required, the sampling size can always be increased.

C. CALIBRATION TEST OF ANGLE SENSOR

The detection device designed in this paper requires a total of three angle sensors, and each angle sensor has two potentiometers. Due to the installation error of the potentiometer and the limitation of manufacturing precision, it is necessary to correct the 6 potentiometers.

All potentiometers on the three sensors are numbered 1-6. The maximum and minimum values of the potentiometer signal was measured. Then the laser level was used to ensure that the angle sensor was placed in the neutral position. The angle sensor is placed at the position of the ''z-axis'' shown in Fig. 6-a, and the potential at this time was collected. The value of the device was recorded as the median value. At the time of sampling, each group was subjected to 1000 experiments to ensure the accuracy of the values, and the final value was obtained by taking the mean value. The experimental results are shown in Table 2.

The experimental result shows that the value of the angle sensor always has certain fluctuations during sampling, which is caused by the hardware circuit itself. Multiple sampling was performed without changing the resolution and sensitivity of the ADC. The maximum value of each potentiometer was basically stable at 114, the minimum value was 6.5, the median value was about 60, and the variance of each group of data was less than 0.5.

The sensor was calibrated based on the above data and the angle of the sensor was converted to the θ and φ values in the mathematical model. The angle sensor's limit deflection angle selected by the experiment was $-25°$ to $+25°$. Taking the value of θ as an example, if the angle sensor produces the value V, the following relationship can be derived:

$$\theta = \begin{cases} \dfrac{25 \times (V - V_{middle})}{(V_{\max} - V_{middle})} \cdot \dfrac{\pi}{180} (V \geq V_{middle}) \\ \dfrac{25 \times (V - V_{middle})}{(V_{middle} - V_{\min})} \cdot \dfrac{\pi}{180} (V < V_{middle}) \end{cases} \tag{5}$$

$$V_{middle} = \frac{V_{\min} + V_{\max}}{2} \tag{6}$$

where: $V_{\max}$ is the maximum value of the sensor, $V_{\min}$ is the minimum value of the sensor, V_{middle} is the value when the sensor is in the middle position, and V is the current angle value of the sensor. In addition, φ and θ are only different in the yaw axis in the model, and the numerical values are calculated as above.

Since the values of φ and θ in the model pass the sign to indicate the direction of deflection, the direction is determined by the magnitude relationship between the current value V and the median value V_{middle}. In the ideal state, the relationship between $V_{\max}$, $V_{\min}$, and V_{middle} is as shown in Equation (6). However, due to manufacturing and assembly

TABLE 2. Angle sensor parameter collection results.

Sensor number	1	2	3	4	5	6
Number of samples	1000	1000	1000	1000	1000	1000
Average of the maximum	114.286	114.449	114.702	115.392	114.166	115.332
Variance of the maximum	0.434	0.414	0.428	0.531	0.458	0.427
Average of the minimum	6.565	6.945	6.598	6.466	6.569	6.683
Variance of the minimum	0.145	2.597	0.167	0.174	0.147	0.154
Average of median values	63.701	57.891	59.779	58.37	60.176	62.22
Variance of the median value	0.459	0.424	0.399	0.393	0.282	0.370

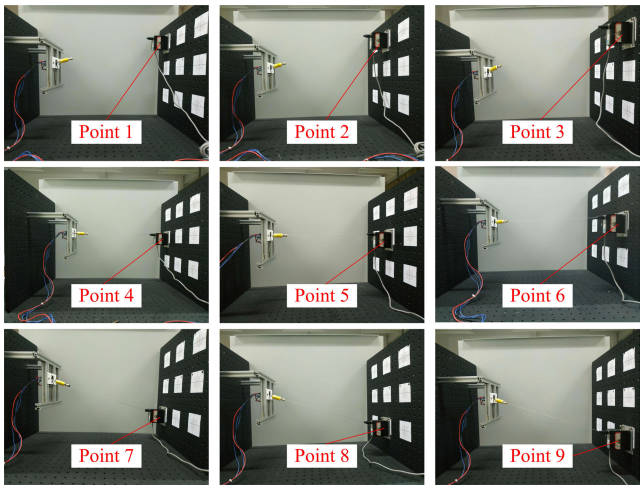

FIGURE 13. Single point detection experimental process diagram.

errors, when the angle sensor is in the mechanical neutral position, it is difficult to ensure that the corresponding potentiometer value V_{middle} is exactly the median value of $V_{\min}$ and $V_{\max}$. Although the above calculation method sacrifices the uniformity of resolution in different directions, it also ensures the overall accuracy to a certain extent.

V. EXPERIMENTAL STUDY OF THE DETECTION SYSTEM

A. EXPERIMENT OF SINGLE POINT DETECTION

The relative position and posture detection device designed in this paper is composed of three angle sensors and three displacement sensors. Each angle sensor was used with one displacement sensor. Therefore, in order to evaluate the accuracy of the measuring device, a single point detection experiment was designed, the accuracy of detecting a single point when one angle sensor was used together with one displacement sensor was determined.

In this experiment, an angle sensor was fixed on the reference plane, and a displacement sensor was sequentially installed in different points on the plane to be tested. The single point detection experimental device is shown in Fig. 6. In Fig. 6-a, the geometric center of the angle sensor is the location of the coordinate origin O. The direction pointed by the coordinate axes of the coordinate system O-xyz is also marked in Fig. 6-a. 9 reference points are marked on the plane to be tested, and the displacement sensors were sequentially mounted in the order of 9 reference points, and the relative positions of the reference points are as shown in Fig. 6-c.

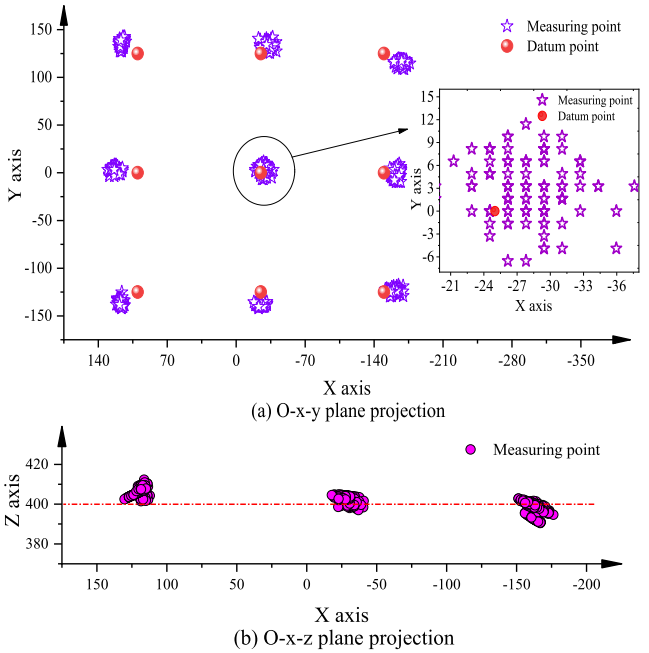

FIGURE 14. Plane projection of single point experiment results.

The test bench was built on the optical platform, and the positioning accuracy of the mounting hole was high, so the coordinates of each reference point were relatively accurate on the plane to be tested. Data in this experiment were acquired from an angle sensor and a displacement sensor through a signal acquisition device. The single point detection experiment process is shown in Fig. 13. In this experiment, 100 sets of experiments are performed for each reference point, and the coordinates of each measurement point are calculated in MATLAB.

The plane projection of the single point experiment results is shown in Fig. 14. Experiment shows that in the o-x-y plane, each measurement point is basically around the datum point, and the measurement point is projected on the o-x-y plane along the positive z-axis as shown in Fig. 14-a; on the o-x-z plane, the data is basically concentrated on the reference of 400 mm. Near the line, the measurement point is projected on the o-x-z plane as shown in Fig. 14-b, and the data acquisition effect is good.

The x, y, and z coordinate values of the measurement points generated when each datum point was measured were taken as the measured value of the datum point, and the distance between the measured value and the datum point

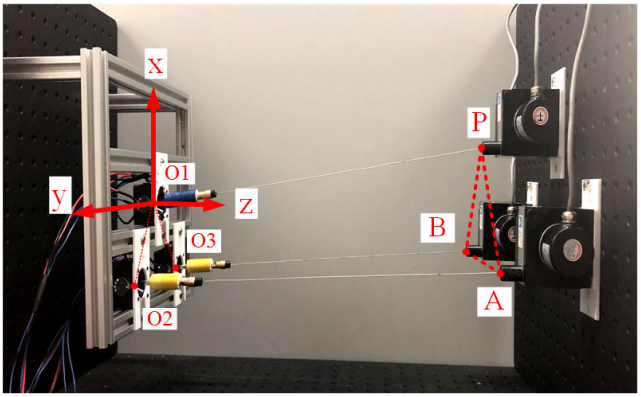

FIGURE 15. Experimental device for three-point detection on the plane.

was calculated. The single point measurement result is shown in Table 3. It can be seen from Table 3 that between each measured value and its datum point, the point with the largest distance is point 4, the distance is 24.28 mm; the point with the smallest distance is point 5, the distance is 5.93 mm.

Considering the actual working environment of the hydraulic support in the coal mine and the size of the hydraulic support, the pose detection device designed in this paper basically meets the measurement requirements.

B. THREE-POINT DETECTION EXPERIMENT ON THE PLANE

Only a relative position of a point on the plane can be obtained by a single point experiment. Therefore, in order to further obtain the relative position and posture, a three-point detection on the plane test is required. The experimental device for three-point detection on the plane is shown in Fig. 15. Since the angle sensor changes angle during installation, to keep with the parameters in the previous experiment, the direction of each coordinate axis of the coordinate system was adjusted. The adjustment does not affect the result.

In this experiment, the three angle sensors were fixed on the same reference plane. And the geometric center points of the respective angle sensors were the positions of the origins of the respective coordinate systems, which were respectively recorded as O1, O2, and O3. Based on the detection principle described above, a fixed coordinate system O1-x-y-z was established at the position where O1 was located, and coordinates of points O2 and O3 in the coordinate system O1-x-y-z were determined. 3 displacement sensors were installed on the plane to be tested, and the outlets of the cable were respectively recorded as P, A, and B. The test bench was built on the optical platform, and the positioning of the mounting hole was precise. At the same time, the optical level was used to position each component before installation to ensure the relative position of each point was accurate. The basic dimensions of the test bench are shown in Table 4. The experiment collected signals through a signal acquisition device. A total of 20 sets of measurements were performed in this experiment, and the data is processed in MATLAB and real-time 3D images were drawn. At the same time,

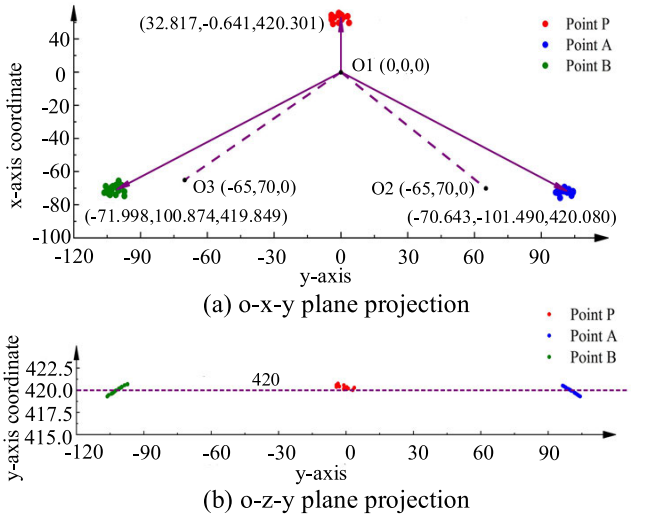

FIGURE 16. Analysis and processing of data.

the coordinates of the points P, A, and B in the space were calculated, a set of data was obtained for each acquisition, and the coordinates of the point calculated were connected with the origin, and the analysis processing of the data is as shown in Fig. 16. The origin shown in Fig. 16 is the point O1 on the experimental setup.

Preliminary observation of the plane formed by the three points P, A, and B shown in the three-dimensional map was basically consistent with the position and posture of the actual plane to be measured. In order to obtain more accurate position and posture information, the coordinates of each mean point were determined by means of multiple sampling and averaging. The analysis results are shown in Fig. 16-a and Fig. 16-b. The position of O1 was taken as the origin of the fixed coordinate system, and the coordinate system O1-xyz is shown in Fig. 15. The two points O2 and O3 were measured in the coordinate system O1. The coordinates measured in the O2 and O3 coordinate systems was converted to the coordinate system O1-xyz. Fig. 16-a and Fig. 16-b shows the projection of each sample point on the O1-x-y plane and the O1-z-y plane. The graph also shows the coordinate mean of the 20 experimental sampling points and the origin position of the coordinate system where the three angle sensors are located. After experimental measurement, the point P, A, and B mounted on the optical platform were located on a vertical plane, which was perpendicular to the z-axis and has a distance of about 420 mm from the point O1. The projections of the point P, A and B on the O1-x-y plane were analyzed. The point A and B are in a horizontal line segment with a distance of 200mm. The point P, A, and B were isosceles triangles, and point P is the apex. The distance between the two points A and B was 100mm. Analysis of the coordinates of each mean point can be concluded that the three-point coordinates detected by the sensor basically conform to the above-mentioned positional features, and the errors are mainly caused by numerical fluctuations and sensor installation errors during the experiment.

TABLE 3. Single point measurement results.

Point	x/mm		y/mm		z/mm		Error (mm)
	Actual value	Measured value	Actual value	Measured value	Actual value	Measured value	
1	100	116.15	125	135.39	400	403.88	19.59
2	-25	-30.98	125	133.92	400	400.31	10.75
3	-150	-167.58	125	115.48	400	398.19	20.07
4	100	123.66	0	2.80	400	404.72	24.28
5	-25	-28.05	0	2.91	400	404.18	5.93
6	-150	-162.74	0	-1.00	400	392.67	14.73
7	100	117.05	-125	-136.57	400	408.45	22.27
8	-25	-25.13	-125	-137.64	400	403.40	13.09
9	-150	-160.47	-125	-123.84	400	399.55	10.55

TABLE 4. Basic dimensions of the test bench.

L_{AB} (mm)	L_{PA} (mm)	L_{PB} (mm)	L_{oo1} (mm)	L_{oo2} (mm)	L_{oo3} (mm)	Distance from point o1 to plane PAB(mm)
200.00	141.42	141.42	0	95.52	95.52	420

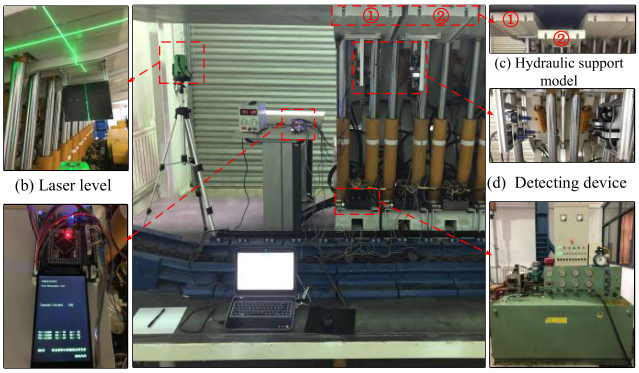

FIGURE 17. Hydraulic support relative position detection test bench.

C. RELATIVE POSITION AND POSTURE DETECTION EXPERIMENT OF HYDRAULIC SUPPORT CANOPY

In order to detect the relative position and posture of the hydraulic support, the canopy is used as the object to be tested, The detecting device is installed at the lower end of the canopy of the adjacent two hydraulic supports, The purpose is to detect the change of the posture of the canopy when the hydraulic support lifting leg. The hydraulic support relative position and posture detection test bench is shown in Fig. 17. At the time of installation, three angle sensors are a group and are installed on the hydraulic support No. 1, and three displacement sensors are a group and are installed on the hydraulic support No. 2. The fixed bracket of the angle sensor is installed at the geometric center of the canopy of the hydraulic support No. 1, and the fixed bracket of the displacement sensor is installed at the geometric center of the canopy of the hydraulic support No. 2.

Fig. 17-a shows the entire experimental system, including: hydraulic support model and its control system, relative position and posture of the detection sensor and signal acquisition module, PC and so on. Among them, the hydraulic support model is a simplified model based on the 8.8 m extra-large height hydraulic support. The support can lift the leg, expand and contract the equilibrium jack, and move the cylinder forward and backward. In order to ensure the installation accuracy during the installation process, the laser level was used for positioning and reducing the influence of the installation angle error on the experimental results. Before the start of the experiment, each hydraulic support was in contact with the top plate and located at the maximum support height. Two hydraulic supports No. 1 and No. 2 were selected as the reference hydraulic support and the hydraulic support to be tested and the posture detecting device is installed.

During the experiment, the height of the leg was gradually reduced from the top position of the hydraulic support, and the x-axis coordinate changes of the points to be measured during the descending process of the leg were collected. The change of each point to be measured as it descends with the leg is shown in Fig. 18. As the leg was lowered, the detected x-axis coordinate values of each point were continuously reduced, which was in line with the action flow of the hydraulic support. At the same time, the x-axis coordinate value of point A was close to the x-axis coordinate value of point B, but as the leg was lowered, the coordinate value of point A was higher than the coordinate value of point B, and the difference between the two points increased. The reason was during the experiment, only the leg of the hydraulic support was lowered, and the length of the equilibrium jack was not adjusted. Therefore, the canopy will have two kinds of movements: the downward translation and the rotation of the hinge point around the link. The front end of the canopy was inclined downward, and the inclination angle was getting larger and larger as the leg was lowered, the x-axis coordinate value of point A will be smaller than point B, and the difference was increased. Further analysis showed that this phenomenon was more obvious after the hydraulic support leg was lowered by 50 mm from the top position.

The projection of the three-point line in the x-o-y plane during the descending of the leg is shown in Fig. 18-b. According to the analysis, the triangle drawn by the connection points

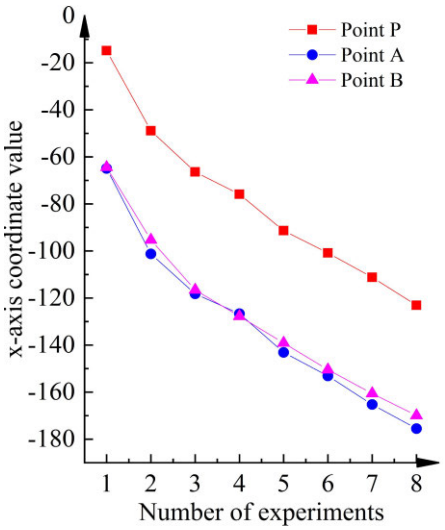

(a) Change of x-axis coordinates of each point

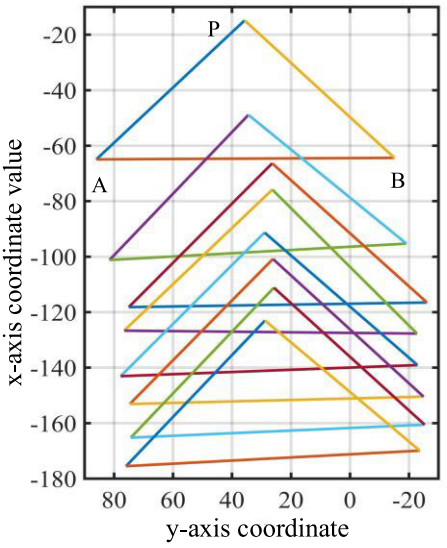

(b) Changes in the x-axis and y-axis coordinates of the three points

FIGURE 18. The change of each point to be measured as it descends with the leg.

of each projection point is closer to the triangle formed by the points P, A, and B in the space, and the triangle drawn by each group of experiments is nearly equal. However, the connection between point A and point B is no longer in a horizontal state. This indicates that the decline of the leg caused the canopy to fall and pitch, but at the same time the canopy also slightly twisted.

A line diagram of the y-coordinate value change of each point is shown in Fig. 19. With the decline of the leg, the y-axis coordinate values of these three points all show a decrease first, then remains stable and has a small up and down fluctuation trend. The movement trend of the three curves is more consistent. It can be found that the leg is not vertically supported upward, but has a certain inclination

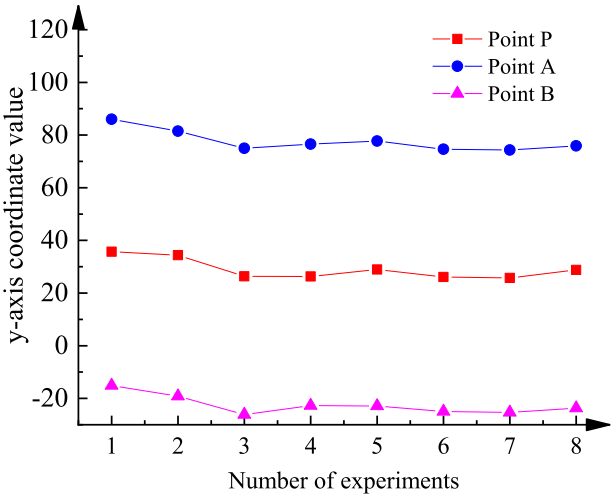

FIGURE 19. Line diagram of the change in the y-axis coordinate value of each point.

angle in the vertical direction. That is, relative to the hinge point on the base, the hinge point on the canopy is more inclined to the side of mining working face. As the leg is lowered, the angle of deflection is reduced, which causes the canopy to move backwards slightly, and the hydraulic support appears as a whole. The phenomenon from the small shift of the center of gravity is consistent with the experimental results.

During the experiment, the points P, A, and B are fixed to move together on the same plane, and the lines of each point in the space always form a right-angled triangle. The area of the right-angled triangle is constant, which is determined when the displacement sensors positions are placed. Therefore, we select 4 parameters to evaluate the sampling accuracy of each sampling point, namely: Distance from point A, B (100 mm), Distance from point P, A (70.7 mm), Distance from point P, B (70.7 mm), Area of the ΔPAB (2500 mm^2). After screening, the points with large errors are eliminated to reduce the error caused by data fluctuation. After the remaining sufficient data is averaged, the parameters calculated by the mean values of each point are shown in Table 5. The above parameters are calculated at each point. They generally meet the experimental requirements.

A line diagram of the z coordinate values of each point, is shown in Fig. 20. Initially, the two points A and B coincide in the z-axis coordinate values, while the P-point value is slightly smaller, This indicates that the canopy plane has a very small angle of roll when the leg is topped, which is negligible; When the leg descends, the coordinate values of the three points are reduced, but the value of point B drops especially fast. And the difference between the two points A and B in the z-axis direction gradually increases, which indicates that the hydraulic support canopy appears twist. As the leg further descends, the difference between the two points of A and B gradually decreases. The value of the final point B changes from the value less than the point A to the value of the point A, which indicates that the torsion direction of the canopy has changed.

TABLE 5. The coordinates of each point are calculated from the mean value.

Number of experiments	Distance from point AB (mm)	Distance from point PA (mm)	Distance from point PB (mm)	Area of the triangular PAB (mm^2)
1	100.841	70.402	70.864	2518.359
2	101.173	71.088	72.628	2494.025
3	99.299	71.546	71.512	2581.410
4	100.713	71.166	70.563	2556.510
5	100.713	71.166	70.563	2510.734
6	99.633	71.341	71.244	2540.578
7	99.854	72.665	71.264	2587.381
8	99.782	70.639	70.576	2492.714

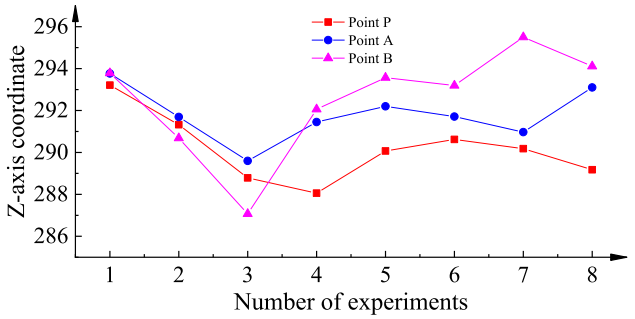

FIGURE 20. Line diagram of the change in the z-axis coordinate value of each point.

The experimental data shows that the twist amplitude of the hydraulic support canopy is small, which is not enough to cause the support to bite each other. The reason for the twist is mainly due to the hinge clearance and structural manufacturing errors during the movement of the support itself.

D. RESULT AND DISCUSSION

In this paper, we discuss the use of angle sensors and displacement sensors to detect relative position and posture on hydraulic supports. In the experimental stage, we successfully used the detection device to detect the relative position and posture of the hydraulic support. The device can detect small posture change of the hydraulic support, and can satisfy the straightness control of the support and the perception of the dangerous posture of the support. In the experiment, the acquisition and transmission of the signal was completed in the field, and the real-time solution of the coordinates was completed on the PC. In the future, we could extend the relative position and posture detection device to the entire mining working face in this way, which helps to realize the overall monitoring of the hydraulic support on mining working face.

Traditional detection methods such as monitoring or machine vision are difficult to apply to the complex coal mine environment, and the reliability of the measurement results cannot be guaranteed. The detection method we use is contact measurement. The measurement result is highly reliable and can reflect the real working state of the hydraulic support.

The detection accuracy of this paper mainly depends on the accuracy of the sensors. The accuracy of the displacement sensor used is high, however, the basic principle of the angle sensor is to use the potentiometer and analog-to-digital conversion circuit, the accuracy of angle sensor is not high. Therefore, the angle sensor can be replaced with an encoder, it will significantly improve the detection stability and detection accuracy.

In addition, the analysis and processing of the data mainly adopts the method of averaging, and the subsequent clustering method can be used to further analyze the relationship between the data.

VI. CONCLUSION

Based on the mathematical idea that three points can determine the plane, we propose a relative position and posture detection method and establishes a detection model. The detection device was developed and the sensors in the device were calibrated experimentally. The detection accuracy was carried out by the single point detection experiment. The test result shows that the accuracy can reach to 24.82 mm. Considering that the height of the hydraulic support is more than 4 m, the accuracy of the detection in this paper is far greater than the traditional manual drawing of the hydraulic support in mining working face, such as pulling the rope or infrared beam. It can basically meet the requirements. At the same time, the position and posture detection and analysis of the hydraulic support descending process were carried out. The result shows that the detection device can detect the relative position and posture of the hydraulic support.

The detection system developed in this paper, under the premise of fully satisfying the detecting requirements to ensure the safe production of coal mines, has a far lower cost than the existing technology. It can create huge economic benefits for the enterprise in the future. At the same time, the research of this paper is of great significance to progress the automatic control of the straightness of mining working face and the perception of the dangerous posture of the hydraulic support, the establishment of an effective method for detecting the instability of the hydraulic support and predicting the inverted frame, and the improvement of the automation and intelligent control level of mining working face.

REFERENCES

[1] J. Wang and Z. Huang, "The recent technological development of intelligent mining in China," *Engineering*, vol. 3, no. 4, pp. 439–444, 2017.
[2] X. T. Zeng, G. Y. Meng, and J. H. Zhou, "Analysis on the pose and dynamic response of hydraulic support under dual impact loads," *Int. J. Simul. Model.*, vol. 17, pp. 69–80, 2018.
[3] Y. Y. Ma, L. Y. Xie, and X. F. Qin, "Strength and reliability analysis of hydraulic support," *Adv. Mater. Res.*, vol. 544, pp. 18–23, 2012.
[4] R. Jonathon, R. David, H. Chad, and H. David, "Sensing for advancing mining automation capability: A review of underground automation technology development," *Int. J. Mining Sci. Technol.*, vol. 24, pp. 305–310, 2014.
[5] C. Luo, X. Fan, J. Ni, H. Yang, X. Zhang, and W. Li, "Positioning accuracy evaluation for the collaborative automation of mining fleet with the support of memory cutting technology," *IEEE Access*, vol. 4, pp. 5764–5775, 2016.
[6] M. E. Yetkin, F. Simsir, M. K. Ozfirat, P. M. Ozfirat, and H. Yenice, "A fuzzy approach to selecting roof supports in longwall mining," *South Afr. J. Ind. Eng.*, vol. 27, pp. 162–177, 2016.
[7] T. Mu-Qin, S. Yi-Bing, and C. Hui-Ying, "One realization method for remote control of hydraulic support of the electro-hydraulic in coal mine face," in *Proc. IEEE 11th Int. Conf. Probabilistic Methods Appl. Power Syst.*, Jun. 2010, pp. 638–641.
[8] S. Hao, S. Wang, R. Malekian, B. Zhang, W. Liu, and Z. Li, "A geometry surveying model and instrument of a scraper conveyor in unmanned longwall mining faces," *IEEE Access*, vol. 5, pp. 4095–4103, 2017.
[9] J. Wang, Z. Wang, X. Jing, T. Chao, and S. Lei, "Moving distance measurement for hydraulic support based on fruit fly optimization algorithm," *Opt. Eng.*, vol. 56, 2017, Art. no. 013111.
[10] Z. Meng, Q. Zeng, K. Gao, S. Kong, P. Liu, and L. Wan, "Failure analysis of super-large mining height powered support," *Eng. Failure Anal.*, vol. 92, pp. 378–391, 2018.
[11] Z. Meng and Q. Zeng, "Pose adjusting simulation of hydraulic support based on mechanical-electrical-hydraulic coordination," *Tehnicki Vjesnik-Tech. Gazette*, vol. 25, pp. 1110–1118, Aug. 2018.
[12] M. Liang, X. Fang, S. Li, G. Wu, M. Ma, and Y. Zhang, "A fiber Bragg grating tilt sensor for posture monitoring of hydraulic supports in coal mine working face," *Measurement*, vol. 138, pp. 305–313, 2019.
[13] J. Xie, X. Wang, S. Hao, and Z. Yang, "Attitude-aware method for hydraulic support groups in a virtual reality environment," *Proc. Inst. Mech. Eng. C, J. Mech. Eng. Sci.*, vol. 233, no. 14, pp. 4805–4818, Jul. 2019.
[14] A. Mura, "Multi-dofs MEMS displacement sensors based on the Stewart platform theory," *Microsyst. Technol.*, vol. 18, pp. 575–579, 2012.
[15] A. Mura, "Sensitivity analysis of a six degrees of freedom displacement measuring device," *Proc. Inst. Mech. Eng. C-J. Mech. Eng. Sci.*, vol. 228, pp. 158–168, Jan. 2014.
[16] C. González-Nicieza, A. Menéndez-Díaz, A. E. Álvarez-Vigil, and M. I. Álvarez-Fernández, "Analysis of support by hydraulic props in a longwall working," *Int. J. Coal Geol.*, vol. 74, pp. 67–92, 2008.
[17] F. Wang, W. Z. Lou, M. R. Guo, and Y. F. Lu, "Intelligent logistics monitoring microsystem based on STM32," *Key Eng. Mater.*, vols. 645–646, p. 4, 2015.
[18] G. Huang and Y. Fan, "Design and realization of vibration signal acquisition & analysis system based on STM32," in *Proc. 28th Chin. Control Decis. Conf.* New York, NY, USA: IEEE, 2016, pp. 2924–2928.
[19] H. Zhang, K. Wei, and J. Procs, "Design of the data acquisition system based on STM32," *Proc. Comput. Sci.*, vol. 17, pp. 222–228, 2013.
[20] J. Zhao, "The design of atmospheric pressure transducer based on the STM32," *Electr. Eng.*, vol. 15, pp. 80–82, 2014.
[21] D. Kim, R. Managuli, and Y. Kim, "Data cache and direct memory access in programming mediaprocessors," *IEEE Micro*, vol. 21, no. 4, pp. 33–42, Jul. 2001.

YI ZHANG was born in 1975. She received the Ph.D. degree from the Beijing Institute of Technology, Beijing, China, in 2009. Her research interests include electromechanical control, measurement, and control technology.

HONGYANG ZHANG was born in 1995. He received the B.E. degree in mechanical and electronic engineering from the Shandong University of Science and Technology, Qingdao, China, in 2018. His research interests include electro-hydraulic control, relative position, and posture detection of hydraulic support.

KUIDONG GAO received the Ph.D. degree from the China University of Mining and Technology, Xuzhou, China, in 2014. Her research interests include research of mining machinery and equipment, equipment testing, and manufacturing.

WENBO XU was born in 1995. He received the dual bachelor's degree in mechatronic engineering, electronic engineering, and automation from the Shandong University of Science and Technology, Qingdao, China, in 2017, where he is currently pursuing the M.E. degree. His research interests include design and manufacture of mining machinery and virtual prototype simulation, relative position, and posture detection of hydraulic support.

QINGLIANG ZENG received the Ph.D. degree in machine design and theory from the China University of Mining and Technology, in 2000. He is currently a Professor with the Shandong University of Science and Technology and Shandong Normal University. He has participated more than 40 projects funded by the National Sci-Tech Support Plan, National 863 Program, and the Natural Science Foundation of China. He published more than 90 articles as a Principle Person. His research interests include electromechanical integration, condition monitoring and fault diagnosis, and virtual prototype.